Mutation of Tyr^{138} Disrupts the Structural Coupling between the Opposing Domains in Vertebrate Calmodulin†

Hongye Sun,‡ Dan Yin,‡ Laurel A. Coffeen,§ Madeline A. Shea,§ and Thomas C. Squier*,‡

Biochemistry and Biophysics Section, Department of Molecular Biosciences, University of Kansas, Lawrence, Kansas 66045-2106, and Department of Biochemistry, University of Iowa, Iowa City, Iowa 52242-1109

Received March 1, 2001; Revised Manuscript Received June 12, 2001

ABSTRACT: We have used circular dichroism and frequency-domain fluorescence spectroscopy to determine how the site-specific substitution of Tyr^{138} with either Phe^{138} or Gln^{138} affects the structural coupling between the opposing domains of calmodulin (CaM). A double mutant was constructed involving conservative substitution of Tyr^{99} → Trp^{99} and Leu^{69} → Cys^{69} to assess the structural coupling between the opposing domains, as previously described [Sun, H., Yin, D., and Squier, T. C. (1999) *Biochemistry 38*, 12266−12279]. Trp^{99} acts as a fluorescence resonance energy transfer (FRET) donor in distance measurements to probe the conformation of the central helix. Cys^{69} provides a reactive group for the covalent attachment of 5-((((2-iodoacetyl)amino)ethyl)amino)naphthalene-1-sulfonic acid (IAEDANS), which functions as a FRET acceptor and permits the measurement of the rotational dynamics of the amino-terminal domain. These CaM mutants demonstrate normal calcium-dependent gel-mobility shifts and changes in their near-UV CD spectra, have similar secondary structures to wild-type CaM following calcium activation, and retain the ability to fully activate the plasma membrane Ca-ATPase. The global folds, therefore, of both the carboxyl- and amino-terminal domains in these CaM mutants are similar to that of wild-type CaM. However, in comparison to wild-type CaM, the substitution of Tyr^{138} with either Phe^{138} or Gln^{138} results in (i) alterations in the average spatial separation and increases in the conformational heterogeneity between the opposing globular domains and (ii) the independent rotational dynamics of the amino-terminal domain. These results indicate that alterations in either the hydrogen bond between Tyr^{138} and Glu^{82} or contact interactions between aromatic amino acid side chains have the potential to initiate the structural collapse of CaM normally associated with target protein binding and activation.

Calmodulin (CaM)[1] is a calcium sensor that rapidly coordinates intracellular metabolism and energy transduction pathways in response to changes in intracellular calcium concentrations through the modulation of the function of numerous channels, receptors, and enzymes (*1*, *2*). The crystal structure of the calcium-liganded form of CaM contains two structurally homologous globular domains connected by a solvent-exposed central sequence located between Leu^{69} and Phe^{92} that is predominantly α-helical (Figure 1) (*3*, *4*). Upon calcium binding, there are structural changes involving the central sequence and the arrangement of α-helices within both the amino- and carboxyl-terminal domains of CaM that alter the hydrodynamic radius (*5*−*9*). The latter structural rearrangements result in the formation of hydrophobic binding clefts within each globular domain that are critical in promoting CaM association with a range of CaM-binding sequences with little structural homology (*10*−*13*).

Dynamic structural rearrangements involving the central sequence are slow relative to the time-scale of overall protein rotational motion, indicating that the opposing globular domains are structurally coupled prior to association with target proteins (*8*, *14*). Binding of calcium-activated CaM to target proteins normally involves the sequential association of both domains to induce enzyme activation (*15*, *16*). Following target protein association, the central sequence becomes conformationally disordered, permitting the two domains to bind to a range of different target sequences with variable binding sequences (*17*−*20*). Thus, initial binding of the high-affinity carboxyl-terminal domain to the CaM-binding sequence in the target protein induces association of the lower-affinity amino-terminal domain as a result of the increase in its effective concentration (*21*). To identify the mechanisms that function to destabilize the central sequence and induce the structural collapse of CaM around

† Supported by National Institutes of Health Grants AG17996 and GM57001.

* Correspondence should be addressed to this author. Tel: (785)-864-4008; FAX: (785)-864-5321; E-mail: tsquier@ukans.edu.

‡ University of Kansas.

§ University of Iowa.

[1] Abbreviations: CaM, calmodulin; central sequence, solvent-exposed sequence located between Leu^{69} and Phe^{92}; DTNB, 5,5′-dithiobis(2-nitrobenzoic acid); EGTA, ethylene glycol bis(β-aminoethyl ether)-*N*,*N*,*N*′,*N*′-tetraacetic acid; ESI-MS, electrospray ionization mass spectrometry; FRET, fluorescence resonance energy transfer; HEPES, *N*-(2-hydroxyethyl)piperazine-*N*′-2-ethanesulfonic acid; HPLC, high-performance liquid chromatography; HW, full width at half-height of a Gaussian distance distribution; IAEDANS, 5-((((2-iodoacetyl)amino)-ethyl)amino)naphthalene-1-sulfonic acid; MHz, megahertz; r_{app}, apparent distance between donor and acceptor chromophores; r_0, initial anisotropy at time zero; R_{av}, average distance between donor and acceptor chromophores; SDS−PAGE, sodium dodecyl sulfate−polyacrylamide gel electrophoresis; $\langle\tau\rangle$, average fluorescence lifetime; $\bar{\tau}$, mean fluorescence lifetime; ϕ, rotational correlation time.

10.1021/bi0104266 CCC: $20.00
Published on Web 07/12/2001

FIGURE 1: Depiction of backbone fold of calcium-activated CaM. Proximal relationships are depicted between Tyr^{138} and neighboring side chains involved in hydrogen bonding (Glu^{82}) or aromatic contact interactions (Phe^{89} and Phe^{141}) using a ball-and-stick representation. Secondary structural elements involving α-helices (red cylinders), β-sheets (yellow ribbons), and turns (blue elements) are illustrated relative to calcium-binding sites (gray spheres) and donor (Trp^{99}) and acceptor (AEDANS covalently bound to Cys^{69}) chromophores used in distance measurements (white spheres). The extended solvent-exposed central sequence is located between between Leu^{69} and Phe^{92}. Illustration was created using coordinates 3cln.pdb (*3*), where the amino-terminal domain is at the top of the figure.

the binding sequence of the target protein, we have used site-directed mutagenesis in conjunction with CD and fluorescence spectroscopy to investigate the possible importance of Tyr^{138} in mediating the structural coupling between the opposing domains in CaM. Tyr^{138} functions as a hydrogen bond donor in the crystal structure of CaM (Figure 1), and has been suggested to stabilize the interdomain central sequence (*3*, *4*, *22*). Consistent with this suggestion, Tyr^{138} is conserved in all Animalia and in the majority of CaM isoforms expressed in Plantae, Fungi, and Protista with the notable exception of *Saccharomyces cerevisiae*, where CaM assumes a collapsed structure that brings the opposing domains into close proximity (*23*, *24*). However, Tyr^{138} has also been suggested to play a role in stabilizing the carboxyl-terminal domain through aromatic side chain interactions with proximal Phe side chains (e.g., Phe^{89} and Phe^{141}) (*3*, *13*, *22*, *25*). To differentiate the relative roles of the hydrogen bond between Tyr^{138} and Glu^{82} from stabilizing interactions involving aromatic side chains that may also mediate interdomain communication by stabilizing the four-helix bundle in the carboxyl-terminal domain of CaM (*13*, *26*), we have engineered two CaM mutants involving the site-directed mutation of Tyr^{138} to either Phe^{138} or Gln^{138}. In this latter respect, Phe^{138} lacks the hydroxyl group involved in the hydrogen-bonding interaction between Tyr^{138} and Glu^{82}, but is expected to maintain aromatic contact interactions with nearby aromatic side chains. Conversely, mutation of Tyr^{138} to Gln^{138} disrupts aromatic contact interactions that normally occur between Tyr^{138} and surrounding aromatic amino acids, but has the potential to form hydrogen bonds to stabilize interdomain interactions (*27*).

Fluorescence resonance energy transfer (FRET) was used to measure the average spatial separation and conformational heterogeneity between chromophoric groups proximal to the opposing ends of the central helix (*8*). These measurements involve the conservative substitution of $Leu^{69} \rightarrow Cys^{69}$ and $Tyr^{99} \rightarrow Trp^{99}$, which are located in the opposing domains of CaM on opposite sides of the solvent-exposed central sequence between Leu^{69} and Phe^{92}. Trp^{99} both functions as a fluorescent reporter group of structural alterations involving the carboxyl-terminal globular domain and serves as a FRET donor. Cys^{69} permits the covalent attachment of IAEDANS, which functions as a FRET acceptor. Lifetime-resolved fluorescence resonance energy transfer (FRET) measurements permit the resolution of the spatial separation and conformational heterogeneity between these engineered sites. Additional measurements of the solvent accessibility, lifetime, and rotational dynamics of either Trp^{99} or AEDANS bound to Cys^{69} provide complementary information regarding the structural alternations in both the local environment around these chromophores and with respect to the overall dimensions of CaM.

We find that in comparison to wild-type CaM, that the substitution of Tyr^{138} with either Gln^{138} or Phe^{138} results in the structural uncoupling of the opposing globular domains of CaM. However, while substitution of Tyr^{138} with Phe^{138} selectively destabilizes the structure of the central sequence, the opposing domains of CaM remain far apart following calcium activation. In contrast, the substitution of Tyr^{138} with Gln^{138} destabilizes the carboxyl-terminal domain and results in a closer proximity between the opposing domains following calcium activation. These results indicate that the hydrogen bond between Tyr^{138} and Glu^{82} as well as aromatic contact interactions between Tyr^{138} and proximal side chains play important and distinct roles in modulating the structural coupling between the opposing domains. We suggest that alterations in these structural interactions resulting from target protein binding may initiate the structural collapse of CaM around target proteins.

EXPERIMENTAL PROCEDURES

Materials. 5-((((2-Iodoacetyl)amino)ethyl)amino)naphthalene-1-sulfonic acid (IAEDANS) was obtained from Molecular Probes, Inc. (Eugene, OR). WP PEI (weak anion exchanger) packing for the HPLC column was ordered from

J. T. Baker (Phillipsburg, NJ), and the weak-anion exchange column used to purify CaM was packed in-house. A Micro BCA protein assay reagent kit was obtained from Pierce (Rockford, IL). Porcine erythrocyte ghost membranes were prepared at 0 °C in an ice bath, essentially as described by Penniston and co-workers (*28, 29*). Purified CaM and erythrocyte ghost membranes were stored at −70 °C.

Expression and Purification of Calmodulin Mutants. The coding region for chicken CaM [accession number MCCH (PIR database) or P02593 (SWISS−PROT database)] was subcloned into the mutagenesis and expression vector pALTER-Ex1 (Promega, Madison, WI). The recombinant plasmid pEx1-CaM was transformed into *E. coli* strain JM109-(DE3) for overexpression, as previously described (*8, 30*). The sequence of chicken CaM is identical to all other expressed vertebrate CaM, including human, mouse, rat, rabbit, bovine, duck, frog, and salmon (*31*). Furthermore, the measured mass of the expressed chicken CaM obtained using electrospray ionization mass spectrometry (ESI-MS) is 16 707 ± 3 Da, which is in good agreement with the theoretical mass of 16 706.4 Da for the following sequence: ADQLTEEQIA[10] EFKEAFSLFD[20] KDGDGTITTK[30] ELGTVMRSLG[40] QNPTEAELQD[50] MINEVDADGN[60] GTIDFPEFLT[70] MMARKMKDTD[80] SEEEIREAFR[90] VFDKDGNGYI[100] SAAELRHVMT[110] LGEKLTDEE[120] VDEMIREADI[130] DGDGQVNYEE[140] FVQMMTAK[148]. This sequence contains no endogenous cysteines, permitting us to specifically introduce a single cysteine at position 69 for modification with AEDANS. In all cases, site-directed mutagenesis was carried out as described in the technical manual for the Altered Sites II in vitro mutagenesis system (Promega, Madison, WI). The following three constructs were created: (i) CaMCW involved the site-directed substitutions of Leu[69] → Cys[69] and Tyr[99] → Trp[99]; (ii) CaMCWF involved the site-directed substitutions of Leu[69] → Cys[69], Tyr[99] → Trp[99], and Tyr[138] → Phe[138]; (iii) CaMCWQ involved Leu[69] → Cys[69], Tyr[99] → Trp[99], and Tyr[138] → Gln[138]. In all cases, oligonucleotide primers containing the desired mutation were synthesized by Macromolecular Resources (Colorado State University, Ft. Collins, CO). Correct mutations were ensured by automated DNA sequencing performed in the Biochemical Research Service Laboratory (University of Kansas, Lawrence, KS). Overexpressed CaM was purified as previously described using phenyl-Sepharose CL-4B (Pharmacia, Piscataway, NJ) and weak-anion exchange HPLC (*32*). The purity of the expressed proteins was greater than 99% as indicated by SDS−PAGE and ESI-MS.

Protein Concentration Determination and Enzymatic Assay. CaM concentration was typically measured using the micro BCA assay (Rockford, IL), using desalted CaM as a protein standard ($\epsilon_{277\ nm}$ = 3029 M^{-1} cm^{-1}) (*33*). The erythrocyte ghost membrane protein concentration was determined by the method of Biuret (*34*), using BSA as the standard. Rates of ATP hydrolysis of the plasma membrane (PM) Ca-ATPase were determined by measuring phosphate release, as previously described (*35*).

Specific Derivatization of Cys[69] in Genetically Engineered CaM. Prior to chemical derivatization, CaM was incubated in 30 mM HEPES (pH 7.5), 1.0 mM EGTA, and 50 mM DTT at room temperature for 3 h to eliminate possible intermolecular cross-linking. Following the addition of 1.0 mM $CaCl_2$, CaM was bound to a phenyl-Sepharose CL-4B affinity column, and DTT was removed by exhaustively washing the column with 50 mM HEPES (pH 7.5) and 0.1 mM $CaCl_2$. The reduced calmodulin was subsequently eluted from the column in 50 mM HEPES (pH 7.5) and 1.0 mM EGTA. Chemical derivatization of Cys[69] was carried out in the dark, and involved the addition of 60 μM IAEDANS to a solution containing 6 μM calmodulin (0.1 mg/mL) in 30 mM HEPES (pH 7.5), 1 mM EGTA, and 6.0 M guanidine hydrochloride. The reaction was stopped after 4 h by the addition of 1 mM β-mercaptoethanol. CaM was again loaded onto a phenyl-Sepharose CL-4B affinity column, the free probe and β-mercaptoethanol were removed, and the labeled CaM was eluted from the column (see above).

The fraction of AEDANS covalently bound to CaM was determined using the following extinction coefficient: $\epsilon_{336\ nm}$ = 5700 M^{-1} cm^{-1} (*36*), and respective average values of 0.70, 0.95, and 0.92 were obtained for CaMCW, CaMCWF, and CaMCWQ. Chemically derivatized CaM was subsequently lyophilized following exhaustive dialysis against 5 mM ammonium bicarbonate buffer (pH 8.0).

Circular Dichroism (CD) Spectroscopy. Circular dichroism (CD) spectra were measured at 20 °C using a Jasco JB710 spectropolarimeter (Jasco Corp., Tokyo, Japan) and a temperature-jacketed spectral cell with a path length of 1.0 cm using desalted CaM (50 μg/mL) in 20 mM Tris-HCl (pH 7.5), 0.1 M KCl, and 0.1 mM EGTA in the absence and presence of 0.2 mM $CaCl_2$. The α-helical contents of the proteins were determined by a nonlinear least-squares fit using the program Contin (*37*). Temperature-dependent changes in the molar ellipticity at 222 nm were determined for apo-CaM using an Aviv 62DS CD spectrometer equipped with a thermoelectric temperature controller and immersible thermocouple accurate to ±0.4 °C, where the heating rates were 1 °C/min. The data from the thermal denaturation of wild-type and CaM mutants were fit using a two- and three-state unfolding model to obtain transition temperatures and enthalpy values, essentially as previously described (*38, 39*).

Fluorescence Measurements. Steady-state fluorescence spectra were measured using a FluoMax spectra fluorometer (Instruments S. A., Edison, NJ). The emission spectra of Trp[99] were taken by exciting the samples at 297 nm, and the slit width was adjusted to 5 nm on the emission side. The sample contains 3 μM CaM in the buffer containing 0.1 M HEPES (pH 7.5), 0.1 M KCl, and 0.1 mM EGTA in the absence or presence of 0.2 mM $CaCl_2$. Frequency-domain lifetime and anisotropy measurements involved either the 333 nm output from a Coherent Innova 400 argon ion laser (Santa Clara, CA) to excite AEDANS or the tripled output (297 nm) of a Ti:sapphire laser (Coherent, Mira 900) tuned to 891 nm, whose frequency was reduced to 5 MHz using a Coherent pulse picker (model 9200) to excite tryptophan. The fluorescence lifetime or anisotropy was measured using an ISS-K2 fluorometer (Urbana-Champaign, IL), whose design has previously been described in detail elsewhere (*40, 41*). The emitted fluorescence intensity for lifetime or anisotropy measurements of Trp or AEDANS were respectively detected after a monochromator centered at 346 nm (8 nm band-pass) or a Schott long-pass GG400 filter.

Analysis of Frequency-Domain Data. The time-dependent decay, $I(t)$, of any fluorophore can be described as a sum of exponentials:

$$I(t) = \sum_{i=1}^{n} \alpha_i e^{(-t/\tau_i)} \quad (1)$$

where α_i are the preexponential factors, τ_i are the excited-state decay times, and n is the number of exponential components required to describe the decay. Explicit expressions have been provided that permit the ready calculation of α_i and τ_i (*42*). The parameter values were determined by minimizing the χ_R^2 (the F statistic), which serves as a goodness-of-fit parameter that provides a quantitative comparison of the adequacy of different assumed models (*43*). Data were fit using the method of nonlinear least squares to a sum of exponential decays (*44*). After the measurement of the intensity decay, one typically calculates the mean lifetime, $\bar{\tau}$, which is weighted by the amplitudes associated with each of the preexponential terms:

$$\bar{\tau} \equiv \sum_i \alpha_i \tau_i \quad (2)$$

where $\bar{\tau}$ is directly related to the quantum yield of the fluorophore (*45*). Alternatively, to determine the bimolecular quenching efficiency, the average lifetime ($\langle\tau\rangle$) provides a measure of the time that the excited state is available for quenching, where:

$$\langle\tau\rangle = \frac{\sum_i^n \alpha_i \tau_i^2}{\sum_i^n \alpha_i \tau_i} \quad (3)$$

For the case of fluorescence resonance energy transfer (FRET) measurements, more realistic physical models were used involving a distribution of distances (see below), as previously described (*8*, *14*, *46*, *47*).

Calculation of Molecular Distances Using FRET. The efficiencies of energy transfer, E, and the apparent donor−acceptor distance, r_{app}, are calculated from the Förster equations (*48*, *49*), where:

$$E = 1 - \frac{F_{da} - F_d(1 - f_a)}{F_d \times f_a} = 1 - \frac{\bar{\tau}_{da} - \bar{\tau}_d(1 - f_a)}{\bar{\tau}_d \times f_a} = \frac{R_o^6}{R_o^6 + r^6} \quad (4)$$

F_{da} and F_d or $\bar{\tau}_{da}$ and $\bar{\tau}_d$ are the steady-state fluorescence intensities and mean fluorescence lifetimes of Trp^{99} in the presence and absence of the FRET acceptor AEDANS. R_o is the Förster critical distance that defines the distance for a given donor−acceptor pair where the efficiency of FRET is 50%. f_a is the fractional labeling of the acceptor. R_o is given by

$$R_o = (9.79 \times 10^{-5})(n^{-4}\kappa^2\phi_d J)^{1/6} \text{ in cm} \quad (5)$$

where n is the refractive index, κ^2 is the orientation factor, J is the overlap integral, and ϕ_d is the quantum yield of the donor in the absence of acceptor. In our experiments, n is estimated to be 1.40 (*48*); κ^2 is assumed to be 2/3, which assumes that donor and acceptor chromophores undergo rapid isotropic rotational motion compared with the lifetime of the donor (see below); ϕ_d is determined by numerical integration of the fluorescence emission spectrum of Trp^{99} in CaM, using L-tryptophan in 20 mM MOPS (pH 7.0) as a standard, which has a quantum yield of 0.14 (*50*, *51*); J is calculated by numerical integration from the fluorescence emission spectrum of Trp^{99} in CaM and the absorption spectrum of AEDANS bound to Cys^{69} in CaM. Color effects relating to the wavelength-dependent properties of the photomultiplier were corrected using an algorithm provided by ISS Inc. (Urbana-Champaign). In the presence of saturating calcium (pH 7.5), the quantum yield (ϕ_d) for Trp^{99} in CaMCW is 0.098, and the overlap integral, J, for Trp^{99} to AEDANS bound to Cys^{69} is 9.0 ± 10^{-15} M^{-1} cm^3. These constants were remeasured for all CaM mutants under the different experimental conditions used in this study, and are reflected in the measured values of R_0.

The above analysis assumes a unique donor−acceptor separation in the calculation of molecular distances, and ignores any conformational heterogeneity associated with the molecular dynamics of CaM. However, the intensity decay associated with the donor in the presence of an acceptor permits one to recover the conformational heterogeneity (or distribution of distances) associated with CaM (*46*, *52*, *53*). If a single acceptor is present at a distance r from a donor, then the transfer rate is given by

$$k_{T_i} = \frac{1}{\tau_{D_i}}\left(\frac{R_o}{r}\right)^6 \quad (6)$$

where R_o is the Förster distance. If a single D−A pair is separated by a fixed distance r, the intensity decay is given by

$$I_{DA}(r,t) = \sum_{i=1}^{n} \alpha_{D_i} \exp(-t/\tau_{DA_i}) \quad (7)$$

where the individual decay times observed in the presence of the energy transfer acceptor are

$$\frac{1}{\tau_{DA_i}} = \frac{1}{\tau_{D_i}} + \frac{1}{\tau_{D_i}}\left(\frac{R_o}{r}\right)^6 \quad (8)$$

One generally does not observe a unique D−A separation in biomolecules, but rather an average determined by the probability distance distribution, $P(r)$ (*53*). A distribution of D−A separations is expected from measurements of molecular dynamics of a range of proteins, as well as statistical mechanical simulations that indicate the presence of conformational heterogeneity associated with long polymers (*43*). The latter calculations indicate that long polymers can be adequately described using Gaussian distribution functions. Hence, the observed intensity decay is

$$I_{DA}(t) = \int_{r=0}^{\infty} P(r) \sum_{i=1}^{n} \alpha_{D_i} \exp\left[-\frac{t}{\tau_{D_i}} - \frac{t}{\tau_{D_i}}\left(\frac{R_o}{r}\right)^6\right] dr \quad (9)$$

It should be noted that the proper choice of boundary conditions ensures that physically unrealistic donor−acceptor separations (i.e., $r < 0$) are not allowed. Therefore, if part of the Gaussian distribution [$P(r)$] contains distances less than zero, then the integral [i.e., $\int P(r)\,dr$] is less than unity. This type of truncated Gaussian distance distribution has previously been observed for staphylococcal nuclease, melittin, thiopeptides, and denatured troponin I (*47*, *54*−*56*).

Our objective is to recover $P(r)$ from the intensity decay. To minimize the number of parameters, a uniform Gaussian distribution of donor to acceptor distances is generally assumed:

$$P(r) = \exp\left[-\frac{1}{2}\left(\frac{r - R_{av}}{\sigma}\right)^2\right] \quad (10)$$

where R_{av} is the average distance and σ is the standard deviation of the distribution. The width of the distribution is reported as the full-width at half-maximum (half-width, hw), which is given by hw = 2.354 σ. For analysis in terms of a sum of exponentials, we used the analytical forms of N_ω and D_ω previously described (*41*−*43*), using the Globals software package (University of Illinois, Urbana-Champaign). For the distance distributions, we used numerical integration to calculate:

$$N_\omega = \int_{r=0}^{\infty} \sum_{i=0}^{n} \frac{P(r)\omega\tau_{DA_i}^2}{1 + \omega^2\tau_{DA_i}^2}\,dr \text{ and } D_\omega = \int_{r=0}^{\infty} \sum_{i=1}^{n} \frac{P(r)\tau_{DA_i}}{1 + \omega^2\tau_{DA_i}^2}\,dr \quad (11)$$

using software provided by the Center for Fluorescence Spectroscopy (Baltimore, MD). The adequacy of the Gaussian model is assessed through a comparison of the goodness of the fit (i.e., χ_R^2; see below) relative to the fit using the more general multiexponential model which assumes no physical model.

Decays of Fluorescence Anisotropy. As previously described, time-resolved anisotropies were measured using the differential phase ($\Delta_\omega = \phi_\perp - \phi_\parallel$) and modulated anisotropy [$r_\omega = (\Lambda_\omega - 1)/(\Lambda_\omega + 2)$], where $\Lambda = m_\parallel/m_\perp$(*43*, *57*). The parameters describing the anisotropy decay were obtained from a least-squares fit to a multiexponential model, where

$$r(t) = r_o \sum_{i=1}^{n} g_i e^{-t/\varphi_i} \quad (12)$$

r_o is the limiting anisotropy in the absence of rotational diffusion, ϕ_i are the rotational correlation times, $r_o \times g_i$ are the amplitudes of the total anisotropy loss associated with each rotational correlation time, and n is the total number of components associated with the exponential decay. The goodness of fit was determined through a comparison of the deviations between the measured and calculated values. Errors in Δ_ω and Λ_ω were assumed to be 0.2 and 0.005, respectively.

RESULTS

Rationale for CaM Mutants. Mutations in CaM involving the site-directed substitution of Leu^{69} → Cys^{69} and Tyr^{99} → Trp^{99} (i.e., CaMCW) do not affect CaM function and were previously used to assess calcium-dependent structural changes involving the spatial arrangement of the opposing globular domains (*8*, *32*). To investigate the suggested role of Tyr^{138} in mediating interdomain communication (*3*, *22*, *25*), we have used site-directed mutagenesis to introduce additional mutations involving the substitution of Tyr^{138} → Phe^{138} (CaMCWF) and Tyr^{138} → Gln^{138} (CaMCWQ). All CaM species were expressed in *E. coli* and purified using the calcium-dependent changes in the hydrophobic interactions between CaM and phenyl-Sepharose CL-4B followed by weak anion exchange HPLC (*33*, *58*). Both CaMCWQ and CaMCWF fully activate the PM-Ca-ATPase at saturating CaM concentrations (data not shown), indicating that these mutations do not alter CaM function under equilibrium conditions.

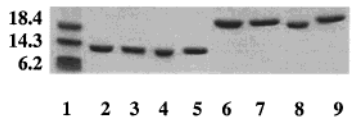

FIGURE 2: Calcium-dependent alterations in the electrophoretic mobilities of CaM. Calcium-activated (lanes 2−5) and apo-CaM (lanes 6−9) for wild-type cloned CaM (lanes 2 and 6), CaMCW (lanes 3 and 7), CaMCWF (lanes 4 and 8), and CaMCWQ (lanes 5 and 9). Experimental conditions involved either 1 mM $CaCl_2$ or 1 mM EGTA using SDS−PAGE [15% (w/v) acylamide]. Molecular mass standards are shown in lane 1.

Electrophoretic Mobility of CaM Mutants. Calcium-dependent alterations in the electrophoretic mobility of CaM using SDS−PAGE have commonly been used to determine whether site-directed mutations alter the structure of CaM (*59*−*61*). Therefore, we have compared the mobility of apo- and calcium-saturated CaMCW, CaMCWF, and CaMCWQ with that observed for wild-type CaM expressed in *E. coli* (Figure 2). Although prior to calcium activation there is a small increase in the electrophoretic mobility of CaMCWF relative to either wild-type CaM or the other CaM mutants, it is apparent that all four samples undergo similar calcium-dependent increases in electrophoretic mobilities that are indicative of normal conformational changes associated with calcium activation.

Circular Dichroism. Additional resolution of possible alterations in CaM structure is possible through a consideration of the near-UV CD spectra, which have previously been shown to provide a sensitive indication of alterations in packing interactions involving Tyr^{138} and other aromatic amino acids, which stabilize the structure of CaM (*62*). In wild-type CaM, there is a major calcium-induced change in the CD spectra centered near 280 nm, which is associated with Tyr^{99} and Tyr^{138} (Figure 3A). The calcium-dependent spectral change associated with CaMCW is similar to wild-type CaM near 280 nm (Figure 3B); additional intensity results from the broader and more intense signals associated with Trp^{99}, which is particularly apparent at wavelengths below 280 nm. Similar calcium-dependent changes are apparent for CaMCWF and CaMCWQ (Figure 3), suggesting that all three CaM mutants undergo similar calcium-dependent structural changes in the vicinity of Trp^{99}.

To assess possible secondary structural differences resulting from the substitution of Tyr^{138} with either Phe or Gln, we have measured the far-UV CD spectra for the three mutants and wild-type CaM. At 20 °C, there are no

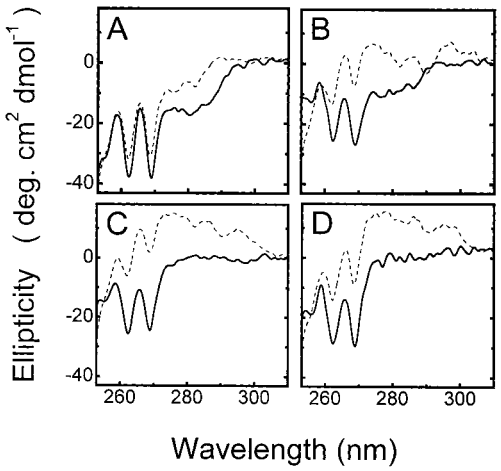

FIGURE 3: Calcium-dependent conformational changes involving aromatic amino acid residues. Near-UV CD spectra of apo- (dashed line) and calcium-activated (solid line) wild-type CaM (A), CaMCW (B), CaMCWF (C), and CaMCWQ (D). Experimental conditions involved 40 μM CaM in 20 mM Tris-HCl (pH 7.5), 0.1 M KCl, and 1 mM EGTA in the absence or presence of 2 mM $CaCl_2$. Temperature was 20 °C.

Table 1: α-Helical Content and Line-Shape Parameters Obtained from Circular Dichroism Spectra of the Apo-Form of Wild-Type and Mutant CaMs[a]

	α-helical content[b]		$\theta_{208}/\theta_{222}$[c]	
sample	+calcium	+EGTA	+calcium	+EGTA
CaM	68 ± 3	66 ± 2	1.03 ± 0.02	1.06 ± 0.01
CaMCW	66 ± 3	63 ± 2	0.99 ± 0.02	1.03 ± 0.01
CaMCWF	64 ± 2	67 ± 2	0.94 ± 0.02	0.95 ± 0.01*[d]
CaMCWQ	62 ± 3	37 ± 3	1.08 ± 0.02	1.36 ± 0.01*

[a] Average values and standard deviations obtained from CD spectra of 3.0 μM wild-type or mutant CaMs in 20 mM Tris (pH 7.5), 0.1 M KCl, and 0.1 mM EGTA at 20 °C. [b] α-Helical content was estimated using the method of ridge regression by the program Contin, as previously described (*8*, *37*, *75*, *76*). [c] Ratio of molar ellipticities at 208 and 222 nm provides a sensitive indication of structural interactions between neighboring helices (*77*). [d] Asterisks indicate statistically significant differences relative to wild-type CaM obtained using the Student's *t*-test (*78*).

substantial differences in the CD spectra following calcium activation, as evidenced by the similar ratios of the molar ellipticities (i.e., $[\Theta_{208}]/[\Theta_{222}]$) or calculated α-helical contents for CaMCW, CaMCWF, or CaMCWQ relative to wild-type CaM (Table 1). These results indicate that following calcium activation neither the backbone fold nor the helical packing interactions are significantly affected by the site-specific substitution of Tyr^{138} with either Phe^{138} or Gln^{138} (*63*, *64*). Likewise, similar CD spectra are observed for the apo-forms of CaMCW and CaMCWF relative to wild-type CaM. There is a small decrease in $[\Theta_{208}]/[\Theta_{222}]$ for apo- and calcium-activated CaMCWF relative to wild-type CaM that suggests alterations in helix packing interactions, which are analogous to observed spectral changes resulting from a reduction in ionic strength for wild-type CaM (*8*). However, in comparison to wild-type CaM, there is a substantial reduction in the α-helical content of apo-CaMCWQ at 20 °C that arises as a result of a large reduction in thermal stability (Figure 4). This latter result is consistent with the proposed role of Tyr^{138} in stabilizing the four-helix bundle in the carboxyl-terminal domain through contact interactions involving neighboring aromatic side chains (*13*).

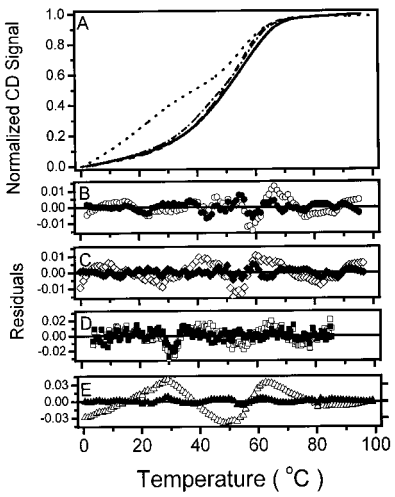

FIGURE 4: Temperature-dependent unfolding of wild-type and CaM mutants. (A) Temperature-dependent ellipticity changes measured at 222 nm and corresponding nonlinear least-squares fits assuming a three-state unfolding process for wild-type CaM (solid line), CaMCW (dashed line), CaMCWF (dot−dashed line), and CaMCWQ (dotted line). Residuals represent differences between experimental data and nonlinear least-squares fits assuming models involving a two-state (open symbols) and three-state (closed symbols) unfolding transition for wild-type CaM (B), CaMCW (C), CaMCWF (D), and CaMCWQ (E) (*39*). Experimental conditions involved 3 μM CaM in 20 mM Tris-HCl (pH 7.5), 0.1 M KCl, and 1 mM EGTA using a heating rate of 1 °C/min.

Table 2: Thermal Unfolding of the Apo-Form of Wild-Type and CaM Mutants[a]

sample	T_1 (°C)	ΔH_1 (kcal/mol)	T_2 (°C)	ΔH_2 (kcal/mol)
wild-type CaM	49 ± 1	28 ± 2	62 ± 1	47 ± 2
CaMCW	49 ± 1	25 ± 4	58 ± 1	42 ± 2
CaMCWF	43 ± 1	33 ± 3	59 ± 1	58 ± 4
CaMCWQ	24 ± 1	17 ± 1	57 ± 1	49 ± 1

[a] Thermal unfolding measurements were performed as described in the legend to Figure 4, and data were fit to a three-state model for unfolding, essentially as previously described (*39*).

Additional insight with respect to the role of Tyr^{138} in modulating the structure of apo-CaM is possible from a consideration of nonlinear least-squares fits of the thermal denaturation curves (Figure 4). In all cases, the unfolding transitions require a three-state model as previously documented for wild-type CaM (*39*). Small decreases in the transition temperatures associated with thermal unfolding are observed for CaMCW and CaMCWF relative to wild-type CaM, indicating that these mutations disrupt localized interactions that normally stabilize the structure of CaM. In contrast, there is a 25 ± 2 °C decrease in the temperature associated with the initial thermal transition (T_1) associated with CaMCWQ (Table 2). No corresponding large changes are apparent in the temperature of the secondary thermal transition (T_2), suggesting that the disruption of aromatic contact interactions involving Tyr^{138} selectively destabilizes the carboxyl-terminal domain without significantly affecting the thermal unfolding of the amino-terminal domain. Alternatively, alterations in the structural coupling between the opposing domains in CaMCWQ may result in the more facile formation of a molten globule state involving both domains.

Steady-State Fluorescence. One observes that the steady-state fluorescence intensities of Trp^{99} are very similar in CaMCW, CaMCWF, and CaMCWQ following calcium

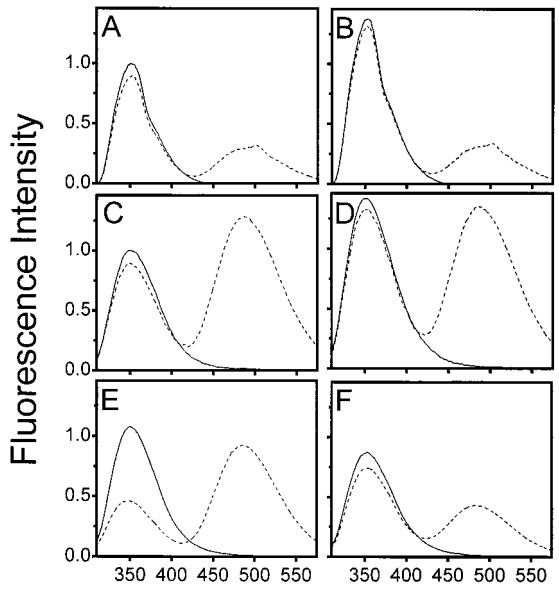

FIGURE 5: Spatial separation between Trp^{99} and AEDANS covalently bound to Cys^{69}. Steady-state fluorescence emission spectra for Trp^{99} (donor) in the absence (solid line) and presence (dotted line) of AEDANS (acceptor) covalently bound to Cys^{69} for calcium-activated (A, C, and E) and apo-CaM (B, D, and E) using CaMCW (A, B), CaMCWF (C, D), and CaMCWQ (E, F). Experimental conditions involved 3 μM CaM in 0.1 M HEPES (pH 7.5), 0.1 M KCl, 0.1 mM EGTA in the absence and presence of 0.2 mM $CaCl_2$ at 20 °C. Excitation was at 297 nm, and emission was detected after a Schott KV-320 long-pass filter; a bandwidth of 5 nm was used for both excitation and emission monochromators. Data for CaMCW were obtained from ref (*8*).

activation (Figure 5; Table 3). However, while calcium activation results in a 30% reduction in the quantum yield of Trp^{99} in CaMCW and CaMCWF, there is a corresponding 25% increase in the quantum yield of Trp^{99} in CaMCWQ following calcium activation. These differences in the quantum yields of Trp^{99} in the apo-form of CaMCWQ relative to that observed for CaMCW or CaMCWF are reflected in similar differences in the mean fluorescence lifetimes ($\bar{\tau}$; see below), and suggest that protein structural changes occur in the vicinity of Trp^{99}. This interpretation is consistent with observed structural differences in apo-CaMCWQ relative to wild-type CaM observed using CD spectroscopy, and indicates that dynamic structural measurements of this sample will reflect multiple effects relating to the decreased conformational stability. However, measurements of apo- and calcium-activated CaMCW and CaMCWF as well as the calcium-activated form of CaMCWQ will permit a quantitative assessment of dynamic structural changes resulting from the loss of specific noncovalent interactions involving Tyr^{138} that may modulate interdomain interactions.

Fluorescence Lifetime Measurements. Changes in the preexponential amplitudes (i.e., α_i) of the three major fluorescence lifetimes (τ_i) associated with individual tryptophans in proteins can reveal additional details regarding localized secondary structural changes, as the relative contribution of different tryptophan rotomers has been demonstrated to be differently constrained by side-chain interactions within different protein secondary structures (*65, 66*). We have, therefore, measured the fluorescence lifetime intensity decay of Trp^{99} in all three CaM mutants using frequency-domain fluorescence spectroscopy (Figure 6). The intensity decays of Trp^{99} for all three mutants can be adequately described as a sum of three exponentials, as indicated by the weighted residuals that are randomly distributed about the origin. Following calcium activation, the fluorescence intensity decays and associated lifetime parameters obtained from a nonlinear least-squares fit to the data are similar for CaMCW, CaMCWF, and CaMCWQ (Table 3). Likewise, the fluorescence intensity decays of the apo-forms of CaMCW or CaMCWF are virtually identical. These results indicate that the secondary structures in the vicinity of Trp^{99} are very similar. In contrast, there are substantial differences in the fluorescence intensity decay of the apo-form of CaMCWQ in comparison to either CaMCW or CaMCWF. The shorter lifetime parameters and large changes in the preexponential amplitudes associated with the apo-form of CaMCWQ reflect differences in the conformational constraints of Trp^{99}, which are consistent with observed differences in the steady-state emission spectra (Figure 5). In summary, the time-dependent intensity decays of Trp^{99} indicate that, irrespective of calcium binding, the backbone fold of CaMCWF is essentially unchanged in the vicinity of Trp^{99} and that there are global structural changes in apo-CaMCWQ that are largely abolished following calcium activation.

Spatial Separation between Trp^{99} and AEDANS Bound to Cys^{69}. To investigate possible alterations in the spatial arrangement of the opposing globular domains that may result from the site-specific mutation of Tyr^{138} to Phe^{138} or Gln^{138}, we have measured the average spatial separation and conformational heterogeneity between the opposing domains using chromophores that have overlapping absorption and fluorescence emission spectra. Trp^{99} serves as a fluorescence resonance energy transfer (FRET) donor, while AEDANS covalently bound to Cys^{69} acts as a FRET acceptor (Figure 1). Following AEDANS modification, CaM is able to fully activate the plasma membrane Ca-ATPase and undergoes normal calcium-dependent structural changes, suggesting that AEDANS labeling results in minimal structural or functional perturbations (*8, 32*). Furthermore, the solvent accessibilities of both AEDANS and Trp^{99} to the collisional quencher acrylamide are very similar for all three CaM samples, irrespective of the substitution of either Phe or Gln for Tyr^{138} (data not shown). These results indicate that there are no significant differences in the tertiary structures in the vicinities of these spectroscopic probes. In the calculation of the apparent spatial separation (r_{app}) between the opposing ends of the central sequence, we have assumed that the orientation between donor and acceptor chromophores is motionally averaged (i.e., $\kappa^2 = 2/3$). As previously discussed, the multiple absorption and transition dipoles and small steady-state polarization values associated with AEDANS bound to Cys^{69} in CaM coupled with the rapid rotational dynamics of these solvent-exposed chromophores suggest that errors in the calculation of distances between Trp^{99} and AEDANS bound to Cys^{69} are no larger than 3 Å (*8, 46, 53, 54*).

In all cases, the covalent modification of Cys^{69} with AEDANS results in FRET, as indicated by decreases in (i) the fluorescence intensity ($\lambda_{em} \approx 350$ nm), (ii) the average lifetime of Trp^{99} (as indicated by the shift in the frequency response toward higher frequencies), and (iii) the stimulated emission of the covalently bound AEDANS chromophore

Table 3: Lifetime Data for Trp^{99} in the Absence and Presence of the FRET Acceptor AEDANS[a]

sample[b]	ligand	label	α_1	τ_1 (ns)	α_2	τ_2 (ns)	α_3	τ_3 (ns)	τ (ns)	χ^2_R [c]
CaMCW[d]	+calcium	donor	0.39 ± 0.08	1.3 ± 0.1	0.45 ± 0.05	2.6 ± 0.3	0.16 ± 0.03	8.0 ± 0.5	2.9 ± 0.1	1.6 (3.3)
		D−A	0.44 ± 0.03	1.2 ± 0.1	0.41 ± 0.02	2.5 ± 0.1	0.15 ± 0.01	7.3 ± 0.3	2.6 ± 0.1	1.6 (3.4)
	+EGTA	donor	0.27 ± 0.04	1.1 ± 0.1	0.23 ± 0.07	3.2 ± 0.1	0.50 ± 0.03	5.9 ± 0.1	4.0 ± 0.1	1.5 (1.8)
		D−A	0.29 ± 0.01	1.1 ± 0.1	0.30 ± 0.02	3.8 ± 0.2	0.41 ± 0.01	5.8 ± 0.1	3.8 ± 0.1	1.5 (1.7)
CaMCWF	+calcium	donor	0.17 ± 0.07	0.9 ± 0.4	0.67 ± 0.06	2.0 ± 0.2	0.17 ± 0.01	7.7 ± 0.2	2.9 ± 0.2	1.6 (4.0)
		D−A	0.39 ± 0.15	1.1 ± 0.2	0.46 ± 0.13	2.4 ±" 0.4	0.15 ± 0.01	7.1 ± 0.2	2.6 ± 0.1	2.1 (4.1)
	+EGTA	donor	0.25 ± 0.01	1.1 ± 0.1	0.28 ± 0.01	3.2 ± 0.3	0.47 ± 0.02	6.2 ± 0.1	4.1 ± 0.1	1.7 (2.1)
		D−A	0.26 ± 0.06	1.0 ± 0.1	0.30 ± 0.08	3.0 ± 0.5	0.44 ± 0.05	5.7 ± 0.2	3.7 ± 0.1	3.6 (4.2)
CaMCWQ	+calcium	donor	0.21 ± 0.07	0.5 ± 0.1	0.51 ± 0.05	2.0 ± 0.3	0.28 ± 0.03	7.2 ± 0.4	3.1 ± 0.3	2.3 (8.6)
		D−A	0.46 ± 0.11	0.4 ± 0.2	0.44 ± 0.05	1.5 ± 0.4	0.10 ± 0.02	6.2 ± 0.7	1.5 ± 0.2	2.2 (12.9)
	+EGTA	donor	0.26 ± 0.06	0.4 ± 0.2	0.45 ± 0.04	2.0 ± 0.5	0.29 ± 0.04	5.2 ± 0.7	2.5 ± 0.3	2.2 (6.5)
		D−N	0.33 ± 0.04	0.4 ± 0.1	0.44 ± 0.03	1.9 ± 0.4	0.24 ± 0.05	4.9 ± 0.5	2.1 ± 0.3	1.7 (6.5)

[a] Indicated values and associated standard errors of the mean (in parentheses) for 5−10 independent measurements collected for Trp^{99} in the absence (donor) or presence (D−A) of AEDANS bound to Cys^{69}. [b] Experimental conditions involved 3 μM CaM in 0.1 M HEPES (pH 7.5), 0.1 M KCl, and 0.1 mM EGTA in the presence (+calcium) or absence (+EGTA) of 0.2 mM $CaCl_2$, where the fractional labeling of Cys^{69} with AEDANS was respectively 0.70, 0.95, and 0.92 for CaMCW, CaMCWF, and CaMCWQ. [c] Average value of the reduced chi-squared (χ^2_R) for a two- (in parentheses) and three-exponential fits to the data. [d] Data taken from Sun and co-workers (*8*).

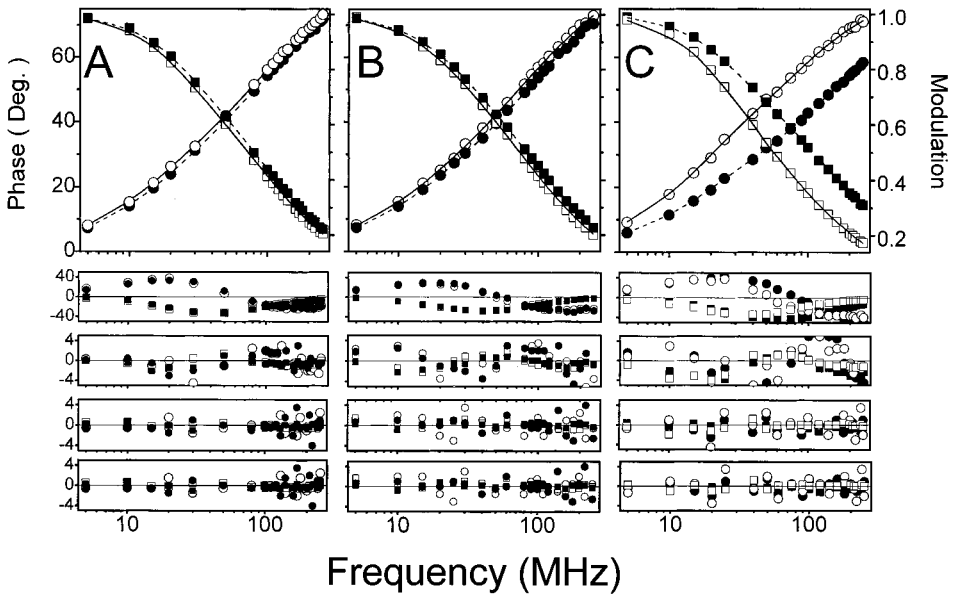

FIGURE 6: Frequency-domain fluorescence lifetime data. Frequency-response of the phase shift (○, ●) or modulation (□, ■) data for Trp^{99} in the absence (○, □) and presence (●, ■) of the FRET acceptor AEDANS covelently bound to Cys^{69} for CaMCW (A), CaMCWF (B), and CaMCWQ (C) following calcium activation. Lines represent nonlinear least-squares fits to a three-exponential fit to the data assuming frequency-independent errors ($\delta_{phase} = 0.2°$; $\delta_{mod} = 0.005$). Lower panels below respective data sets represent the weighted residuals for models involving one-, two-, three-, and four-component fits to the data (top to bottom). Measurements involved 3 μM CaM in 0.1 M HEPES (pH 7.5), 0.1 M KCl, 0.1 mM EGTA, and 0.2 mM $CaCl_2$ at 20 °C Excitation was 297 nm, and emission was detected after a monochromator centered at 346 nm (8 nm band-pass).

($\lambda_{em} \approx 490$ nm) (Figures 5 and 6; Table 3). Similar fluorescence resonance energy transfer efficiencies are calculated using either the reduction in the steady-state intensity or the mean fluorescence lifetime of Trp^{99}, indicating that there is no static component in the measured FRET efficiency that would result from a significant population of chromophores whose donor−acceptor separation is less than $0.5 \times R_o$ (i.e., less than 11 Å). Comparable FRET efficiencies are calculated for CaMCW and CaMCWF, indicating that the opposing domains remain far apart. Likewise, the calculated FRET for CaMCWQ prior to calcium activation suggests that the opposing globular domains remain far apart (Table 4). In contrast, there is a large increase in the FRET efficiency for CaMCWQ following calcium activation (Fig-

Table 4: Spatial Separation between Trp[99] and AEDANS Bound to Cys[69] [a]

sample	ligand	% E [b]	R_o [c] (Å)	r_{app} [d] (Å)	R_{av} [e] (Å)	HW [e] (Å)	χ^2_R [f]
CaMCW	+calcium	15 ± 3	22.6 ± 0.1	30 ± 1	31 (30−33)	1 (0−10)	1.8
	+EGTA	7 ± 1	23.8 ± 0.1	37 ± 2	39 (37−43)	4 (0−15)	2.1
CaMCWF	+calcium	9 ± 1	23.7 ± 0.1	35 ±1	35 (34−37)	16 (11−22)	2.2
	+EGTA	7 ± 1	24.1 ± 0.1	37 ± 2	39 (36−49)	12 (0−28)	2.4
CaMCWQ	+calcium	51 ± 7	23.8 ± 0.1	23 ± 3	21.4 (20.7−21.7)	13 (12−16)	6.8
	+EGTA	16 ± 11	22.2 ± 0.1	29 ± 5	36 (35−37)	28 (23−38)	1.8

[a] Values and associated errors were obtained from 5−10 independent measurements of FRET between Trp[99] and AEDANS bound to Cys[69] using 3 μM CaM in 0.1 M HEPES (pH 7.5), 0.1 M KCl, 0.1 mM EGTA in the presence (+calcium) and absence (+EGTA) of 0.2 mM $CaCl_2$,where the fractional labeling of Cys[69] with AEDANS was respectively 0.70, 0.95, and 0.92 for CaMCW, CaMCWF, and CaMCWQ. [b] Energy transfer efficiencies (E) represent average values and associated standard errors of the mean calculated using lifetime measurements of Trp[99] in Table 3. [c] Förster critical distance (R_o) under the indicated experimental conditions represents the distance between chromophores where the FRET efficiency is 50% (*79, 80*). [d] Apparent distance between Trp[99] and AEDANS bound to Cys[69] calculated assuming a unique conformation. [e] Average donor−acceptor distance (R_{av}) or full-width at half-maximum (HW) assuming a Gaussian distribution of distances (*8, 46, 53*). Indicated errors (in parentheses) were obtained from a global analysis of errors, as depicted in Figure 7. [f] Average value of reduced chi-squared (χ^2_R) fit to Gaussian distribution of distances.

ures 5E and 6C), suggesting that the substitution of Tyr[138] → Gln[138] results in large changes in the spatial arrangement of the opposing globular domains. Under these calcium-saturating conditions, the secondary structure is not significantly affected (Table 1), indicating an important role for aromatic contact interactions between Tyr[138] and surrounding amino acids in the maintenance of the tertiary structure of CaM.

Additional information regarding the average spatial separation and conformational heterogeneity between the opposing globular domains is available from fitting the time-dependent decay of the Trp[99] in the absence and presence of AEDANS to a model that assumes a Gaussian distribution of distances between donor and acceptor chromophores (*8, 32, 46*). The intensity decay of Trp[99] can be adequately described as a sum of three exponentials, as indicated by the random distribution of the weighted residuals about the origin. Inclusion of additional fitting parameters results in no further improvement of χ^2_R. The similar goodness-of-fit (i.e., χ^2_R) obtained when fitting the lifetime data to a model that assumes a Gaussian distribution of distances with two floating parameters (i.e., R_{av} and HW; Table 4) in comparison to the fit obtained using a sum of exponentials with five floating parameters (i.e., α_1, τ_1, α_2, τ_2, and τ_3; Table 3) indicates that fitting the data to the simpler model involving a distribution of distances is statistically justifiable.

As previously described in detail (*8*), two well-defined conformations with narrow half-widths (HW) are observed for CaMCW in the apo-form and following calcium activation, whose respective average donor−acceptor separations (R_{av}) between Trp[99] and AEDANS bound to Cys[69] are 39 and 31 Å (Table 4). The Gaussian distance distributions are significantly different for CaMCWF (R_{av} = 35 Å; HW = 16 Å) and CaMCWQ (R_{av} = 21.4 Å; HW = 13 Å) following calcium activation, as judged by the lack of overlap in the error surfaces for these mutants in comparison to CaMCW (Figure 7A,B). The increase in the HW following mutation of Tyr[138] to either Phe[138] or Gln[138] indicates the presence of increased conformational heterogeneity between the opposing domains of CaM. These results demonstrate that the site-directed substitution of Tyr[138] with either Phe[138] or Gln[138] modulates the structural coupling between the opposing domains in CaM following calcium activation. However, while mutation of Tyr[138] to Phe[138] results in a larger spatial separation (R_{av} = 35 Å), the mutation of Tyr[138] to Gln[138] results in a much smaller spatial separation (R_{av} = 21.4 Å) that brings the opposing domains of calcium-activated CaM into close proximity. Thus, there are substantial differences in the structures of calcium-activated CaM resulting from these latter mutations that respectively disrupt the hydrogen bond between Tyr[138] and Glu[82] (CaMCWF) and aromatic contract interactions that stabilize the tertiary structure of the carboxyl-terminal domain of CaM (CaMCWQ). Similar differential effects resulting from the mutation of Tyr[138] to

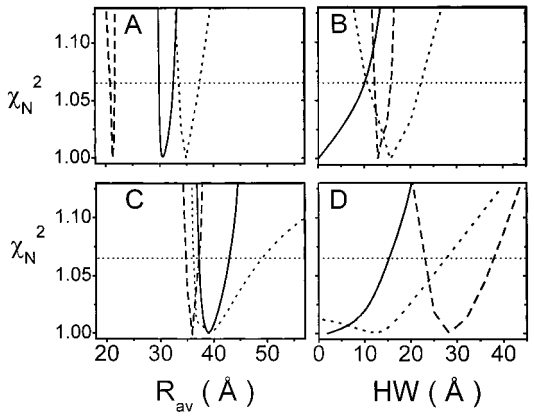

FIGURE 7: Depiction of error surfaces for the Gaussian distance distribution model. Parameter values were obtained from a simultaneous fit using 5−10 data sets to recover the average half-width (HW) and spatial separation (R_{av}) for a Gaussian distribution of distances between Trp[99] and AEDANS covalently bound to Cys[69] in the presence (A, B) or absence (C, D) of 0.2 mM $CaCl_2$, for CaMCW (solid lines), CaMCWF (dotted lines), and CaMCWQ (dashed lines). Experimental values (i.e., R_{av} or half-width) were incrementally adjusted, and all other parameters were allowed to vary in the least-squares analysis, essentially as previously described (*8*). The horizontal dotted line corresponds to the F-statistic for one standard deviation. Experimental conditions are as described in the legend to Figure 5.

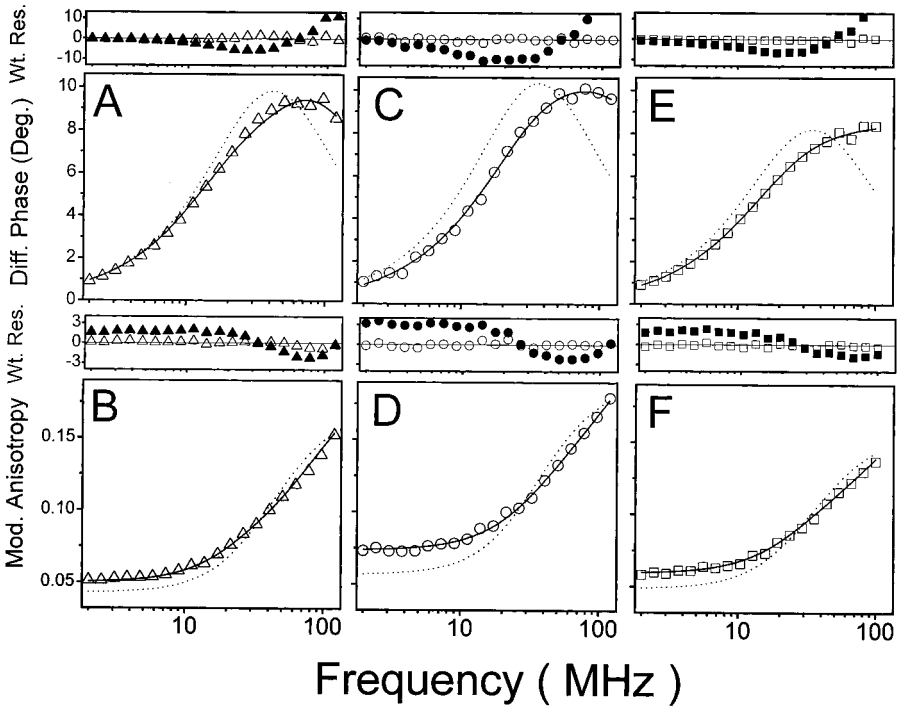

FIGURE 8: Frequency-domain anisotropy data. Differential phase (A, C, and E) and modulated anisotropy (B, D, and F) data for AEDANS covalently bound to Cys[69] in CaMCW (A, B), CaMCWF (C, D), and CaMCWQ (E, F) following calcium activation. Lines represent least-squares fits to one- (dotted line) and two-exponential (solid line) decays, assuming frequency-independent errors ($\delta_{phase} = 0.2°$; $\delta_{mod} = 0.005$). Weighted residuals are shown above each data set for one- (▲, ●, ■) and two-exponential (Δ, ○, □) fits to the data. Experimental conditions are as described in the legend to Figure 5.

Table 5: Rotational Dynamics of AEDANS Bound to Cys[69]

sample	ligand	$\bar{\tau}^a$ (ns)	$g_1 \times r_o{}^b$	$\phi_1{}^b$ (ns)	$g_2 \times r_o{}^b$	$\phi_2{}^b$ (ns)
CaMCW	+calcium	10.9 ± 0.2	0.11 ± 0.01	1.9 ± 0.2	0.08 ± 0.01	12 ± 1
	+EGTA	9.5 ± 0.2	0.12 ± 0.01	1.9 ± 0.3	0.08 ± 0.01	13 ± 2
CaMCWF	+calcium	13.2 ± 0.1*	0.12 ± 0.02	1.3 ± 0.4	0.11 ± 0.02	7 ± 2*
	+EGTA	12.2 ± 0.7*	0.13 ± 0.03	1.5 ± 0.5	0.10 ± 0.02	9 ± 4
CaMCWQ	+calcium	11.6 ± 0.3	0.10 ± 0.01	1.0 ± 0.3*	0.10 ± 0.01	9 ± 1*
	+EGTA	11.4 ± 0.3*	0.10 ± 0.03	1.1 ± 0.2*	0.10 ± 0.01	8 ± 1*

[a] Mean lifetime ($\sum_i \alpha_i \tau_i$) and associated standard errors of the mean for three independent measurements obtained from a three-exponential fit to frequency-domain data collected for AEDANS bound to Cys[69]. [b] Amplitudes ($g_i \times r_o$) and rates (ϕ_i) of rotational motion obtained from two-exponential fits to frequency-domain data, as described in the legend to Figure 8. Errors were obtained from error surfaces associated with simultaneous fits to three independent measurements, where the asterisk indicates statistical differences in parameters relative to CaMCW using *F*-statistic with error surfaces obtained from a global fit to three data sets (*81*).

Phe[138] or Gln[138] are apparent prior to calcium activation. While the site-directed substitution of Tyr[138] with Gln[138] does not significantly affect R_{av} in apo-CaMCWQ, there is a significant increase in the HW of the distance distribution (HW = 28 Å) for CaMCWQ relative to CaMCW (HW < 15 Å). In contrast, the site-directed substitution of Tyr[138] with Phe[138] does not significantly affect either R_{av} or HW in apo-CaM (Figure 7C,D).

Hydrodynamic Properties of CaM. Additional information regarding possible changes in the structural coupling between the opposing globular domains resulting from the site-directed substitution of Tyr[138] with either Phe[138] or Gln[138] is possible through the measurement of the rotational dynamics. We have, therefore, measured the differential phase and modulated anisotropy of AEDANS bound to Cys[69] at 20 frequencies between 2 and 100 MHz (Figure 8). In all cases, the frequency-response of the apo- and calcium-activated forms can be adequately described by two rotational correlation times (Table 5). The longer rotational correlation time observed for CaMCW (i.e., $\phi_2 \approx 12$ ns) has previously been demonstrated to be associated with the global rotational motion of both apo- and calcium-activated CaM (*8*). In contrast, substantially smaller rotational correlation times for ϕ_2 are observed for CaMCWF and CaMCWQ (Figure 9), which are consistent with the uncoupled rotational motion of the amino-terminal domain whose rotational correlation time is expected to be approximately 6−7 ns (*14*, *67*). These latter results indicate that substitution of either Phe or Gln for Tyr[138] results in the structural uncoupling of the opposing globular domains in CaM.

DISCUSSION

Summary of Results. We have demonstrated that substitution of Tyr[138] with either Phe[138] (CaMCWF) or Gln[138] (CaMCWQ) disrupts the structural coupling between the opposing globular domains of CaM, resulting in both the independent rotational motion of the amino-terminal domain and an increase in the conformational heterogeneity between

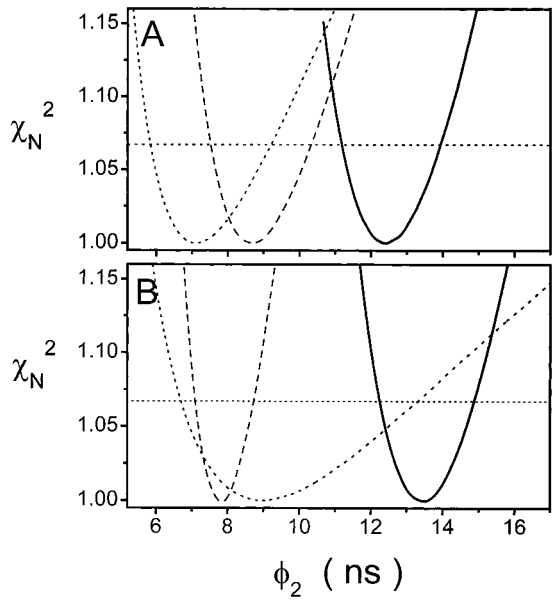

FIGURE 9: Depiction of error surfaces for the rotational dynamics of CaM. Normalized chi-squared values (χ^2_N) resulting from nonlinear least-squares fits following the incremental adjustment of the longer rotational correlation times (ϕ_2) obtained from nonlinear least-squares fits to the data depicted in Figure 8 for CaMCW (thick solid line), CaMCWF (dotted line), and CaMCWQ (dashed line) in the presence (A) or absence (B) of 0.2 mM $CaCl_2$. All other other fitting parameters were allowed to vary. The horizontal dotted line corresponds to the *F*-statistic for one standard deviation. Experimental conditions are as described in the legend to Figure 5.

the opposing domains (Figures 7 and 9). Following calcium activation, the secondary and tertiary structures of both the amino- and carboxyl-terminal domains remain essentially unchanged (Tables 1 and 3). Furthermore, normal calcium-dependent conformational changes involving each of the opposing globular domains are observed (Figures 2 and 3). Thus, the site-directed substitution of Tyr^{138} with either Phe^{138} or Gln^{138} selectively destabilizes the structure of the central sequence located between Trp^{99} and AEDANS bound to Cys^{69} in either CaMCWF or CaMCWQ. These results support earlier suggestions that the hydrogen bond between Tyr^{138} and Glu^{82} and aromatic contract interactions between Tyr^{138} and proximal side chains play important roles in maintaining CaM in an extended conformation (*3*, *22*, *25*), and suggest that calcium binding may modulate interdomain interactions through the stabilization of the structure of the central sequence between Leu^{69} and Phe^{92}.

Relationship to Other Studies. The disruption of the structural linkage between the opposing domains of CaM upon mutation of Tyr^{138} to Phe^{138} is consistent with previous suggestions that the hydrogen bond between Tyr^{138} and Glu^{82} stabilizes the central sequence of CaM (*3*, *4*, *22*). This result is, furthermore, consistent with a range of different measurements involving either site-directed mutagenesis or the oxidative modification of CaM. Thus, the substitution or deletion of Glu^{82} in vertebrate CaM resulted in structural alterations with respect to the overall dimensions of CaM and in the diminished ability of CaM to activate some target proteins (*68*, *69*). Likewise, destabilization of the amphipathic α-helix located between Tyr^{138} and Ala^{147} as a result of the oxidation of Met^{144} or Met^{145} to the corresponding sulfoxide alters the hydrodynamic properties of CaM and results in the structural uncoupling between opposing domains (*25*, *29*, *70*, *71*). This latter result is consistent with observations that the substitution of other bulky amino acids (i.e., either Arg or Val for Met^{145} in vertebrate and paramecium CaM), which would also be expected to destabilize the α-helix between Tyr^{138} and Ala^{147}, respectively, results in an inability to activate either purified phosphodiesterase or the calcium-dependent potassium currents in paramecium (*61*, *72*). Likewise, the substitution of phenylalanine for Tyr^{138} resulted in a reduced binding affinity to the PM-Ca-ATPase (*73*), consistent with a role for Tyr^{138} in mediating important binding interactions necessary for the activation of target proteins.

The modulation of the structural coupling between the opposing domains of CaM by the mutation of Tyr^{138} has important implications with respect to the mechanism of target protein binding. Previous measurements have demonstrated that the initial binding interaction between CaM and target proteins involves the high-affinity association of the carboxyl-terminal domain of CaM followed by association of the amino-terminal domain (*15*, *16*). Association of the amino-terminal domain is aided by the reduced volume available for its diffusion following association of the carboxyl-terminal domain (*16*, *21*). Since the central sequence is disrupted upon binding to target proteins (*17*−*19*), the current results suggest that alterations involving the hydrogen bond between Tyr^{138} and Glu^{82} following initial association of the carboxyl-terminal domain with target proteins may function to mediate the structural collapse of CaM around target sequences.

It should be emphasized that the site-directed substitution of Tyr^{138} with either Phe or Gln does not diminish the ability of these CaM mutants to fully activate the PM-Ca-ATPase. This latter result is consistent with previous observations that the individual domains of CaM are able to fully activate a range of different target proteins, including the PM-Ca-ATPase (*16*, *51*). However, there is a 10-fold reduction in the binding affinity of a CaM mutant involving the site-directed substitution of $Tyr^{138} \rightarrow Phe^{138}$ to the PM-Ca-ATPase (*73*). A similar reduction in binding affinity to the PM-Ca-ATPase is observed upon destabilization of the central helix following deletion of four amino acids (i.e., Met^{145}−Lys^{148}) at the carboxyl-terminus, which results in enhanced interactions between the opposing domains of CaM (*32*). These results suggest that the stabilization of CaM in an extended conformation functions to enhance the binding affinity between CaM and target proteins by diminishing interdomain interactions prior to target protein binding. In addition, maintenance of CaM in an extended conformation has the potential to enhance the kinetics of activation by facilitating the structural collapse of CaM around target sequences. Thus, the marginal stability of the central sequence between Leu^{69} and Phe^{92} in solution may be part of a conformational switch that facilitates target protein activation (*8*, *74*).

Conclusions and Future Directions. We have identified a structural role for Tyr^{138} in stabilizing the central sequence between Leu^{69} and Phe^{92} in CaM, which results in the adoption of an extended structure that minimizes contact interactions between the opposing domains of CaM prior to the association with target enzymes. These results suggest that Tyr^{138} may be part of a conformational switch, such that

the initial association of the carboxyl-terminal domain may trigger the structural collapse of CaM around the CaM-binding sequence of target proteins so as to facilitate enzyme activation. Future studies should aim to (i) identify the influence of interdomain interactions on the kinetics of association and enzyme activation and (ii) quantify other stabilizing interactions critical to the calcium-dependent activation of CaM.

REFERENCES

1. Levitan, I. B. (1999) *Neuron 22*, 645−648.
2. Williams, R. J. P. (1999) in *Calcium as a Cellular Regulator* (Carafoli, E., and Klee, C., Eds.) pp 3−27, Oxford Press, New York.
3. Babu, Y. S., Bugg, C. E., and Cook, W. J. (1988) *J. Mol. Biol. 204*, 191−204.
4. Chattopadhyaya, R., Meador, W. E., Means, A. R., and Quicho, F. A. (1992) *J. Mol. Biol. 228*, 1177−1192.
5. Zhang, M., Tanaka, T., and Ikura, M. (1995) *Nat. Struct. Biol. 2*, 758−767.
6. Finn, B. E., Evenas, J., Drakenberg, T., Waltho, J. P., Thuulin, E., and Forsen, S. (1995) *Nat. Struct. Biol. 2*, 777−783.
7. Sorensen, B. R., and Shea, M. A. (1996) *Biophys. J. 71*, 3407−3420.
8. Sun, H., Yin, D., and Squier, T. C. (1999) *Biochemistry 38*, 12266−12279.
9. Jaren, O. R., Harmon, S., Chen, A. F., and Shea, M. A. (2000) *Biochemistry 39*, 6881−6890.
10. LaPorte, D. C., Wierman, B. M., and Storm, D. R. (1980) *Biochemistry 19*, 3814−3819.
11. Krebs, J., Buerkler, J., Guerini, D., Brunner, J., and Carafoli, E. (1984) *Biochemistry 23*, 400−403.
12. O'Neil, K. T., and DeGrado, W. F. (1990) *Trends Biochem. Sci. 15*, 59−64.
13. Nelson, M. R., and Chazin, W. J. (1998) *Protein Sci. 7*, 270−282.
14. Yao, Y., Schoneich, C., and Squier, T. C. (1994) *Biochemistry 33*, 7797−7810.
15. Persechini, A., Jarrett, H. W., Kosk-Kosicka, D., Krinks, M. H., and Lee, H. G. (1993) *Biochim. Biophys. Acta 1163*, 309−314.
16. Sun, H., and Squier, T. C. (2000) *J. Biol. Chem. 275*, 1731−1738.
17. Meador, W. E., Means, A. R., and Quiocho, F. A. (1992) *Science 257*, 1251−1254.
18. Ikura, M., Clore, G. M., Gronenborn, A. M., Zhu, G., Klee, C. B., and Bax, A. (1992) *Science 256*, 632−638.
19. Meador, W. E., Means, A. R., and Quiocho, F. A. (1993) *Science 262*, 1718−1721.
20. Osawa, M., Tokumitsu, H., Swindells, M. B., Kurihara, H., Orita, M., Shibanuma, T., Furuya, T., and Ikura, M. (1999) *Nat. Struct. Biol. 6*, 819−824.
21. Persechini, A., and Kretsinger, R. H. (1988) *J. Biol. Chem. 263*, 12175−12178.
22. Mukherjea, P., Maune, J. F., and Beckingham, K. (1996) *Protein Sci. 5*, 468−477.
23. Kawasaki, H., and Kretsinger, R. (1995) *Protein Profile 2*, 1070.
24. Lee, S. Y., and Klevit, R. E. (2000) *Biochemistry 39*, 4225−4230.
25. Gao, J., Yin, D. H., Yao, Y., Sun, H., Qin, Z., Schöneich, Ch., Williams, T. D., and Squier, T. C. (1998) *Biophys. J. 74*, 1115−1134.
26. Burley, S. K., and Petsko, G. A. (1985) *Science 229*, 23−28.
27. Richardson, J. S., and Richardson, D. C. (1989) in *Prediction of Protein Structure and the Principles of Protein Conformation* (Fasman, G. D., Ed.) pp 1−98, Plenum Press, New York.
28. Niggli, V., Penniston, J. T., and Carafoli, E. (1979) *J. Biol. Chem. 254*, 9955−9958.
29. Yao, Y., Yin, D., Jas, G. S., Kuczera, K., Williams, T. D., Schoneich, C., and Squier, T. C. (1996) *Biochemistry 35*, 2767−2787.
30. Studier, F. W., and Moffatt, B. A. (1986) *J. Mol. Biol. 189*, 113−130.
31. Putkey, J. A., Ts'ui, K. F., Tanaka, T., Lagrace, L., Stein, J. P., Lai, E. C., and Means, A. R. (1983) *J. Biol. Chem. 258*, 11864−11870.
32. Yin, D., Sun, H., Ferrington, D. A., and Squier, T. C. (2000) *Biochemistry 39*, 10255−10268.
33. Strasburg, G. M., Hogan, M., Birmachu, W., Thomas, D. D., and Louis, C. F. (1988) *J. Biol. Chem. 263*, 542−548.
34. Gornal, A. G., Bardawill, C., and David, M. (1949) *J. Biol. Chem. 177*, 751−766.
35. Lanzetta, P. A., Alverez, L. J., Reinsch, P. S., and Candia, O. (1979) *Anal. Biochem. 100*, 95−97.
36. Haugland, R. P. (1996) *Handbook of Fluorescent Probes and Research Chemicals*, 6th ed., Molecular Probes, Inc., Eugene, OR.
37. Venyaminov, S. Y., and Yang, J. T. (1996) in *Circular Dichroism and the Conformational Analysis of Biomolecules* (Fasman, G. D., Ed.) pp 69−107, Plenum Press, New York.
38. Eftink, M. R., Ionescu, R., Ramsay, G. D., Wong, C.-Y., Wu, J. Q., and Maki, A. H. (1996) *Biochemistry 35*, 8084−8094.
39. Sorensen, B. R., and Shea, M. A. (1998) *Biochemistry 37*, 4244−4253.
40. Gratton, E., and Limkeman, M. (1983) *Biophys. J. 44*, 315−324.
41. Lakowicz, J. R., and Maliwal, B. (1985) *Biophys. Chem. 21*, 61−78.
42. Weber, G. (1981) *J. Phys. Chem. 85*, 943−953.
43. Lakowicz, J. R., and Gryczynski, I. (1991) in *Topics in Fluorescence Spectroscopy* (Lakowicz, J. R., Ed.) Vol. I, pp 293−335, Plenum Press, New York.
44. Bevington, P. R. (1969) *Data Reduction and Error Analysis for the Physical Sciences*, McGraw-Hill, New York.
45. Luedtke, R., Owen, C. S., Vanderkooi, J. M., and Karush, F. (1981) *Biochemistry 20*, 2927−2936.
46. Haas, E., Katchalski-Katzir, E., and Steinberg, I. (1978) *Biochemistry 17*, 5064−5070.
47. Lakowicz, J. R., Gryczynski, I., Cheung, H. C., Wang, C., Johnson, M. L., and Joshi, N. (1988) *Biochemistry 27*, 9149−9160.
48. Fairclough, R. H., and Cantor, C. R. (1978) *Methods Enzymol. 48*, 347−379.
49. Lakowicz, J. R., Gryczynski, I., Wiczk, W., Kusba, J., and Johnson, M. L. (1991) *Anal. Biochem. 95*, 243−254.
50. Chabbert, M., Lukas, T. J., Watterson, D. M., Axelsen, P. H., and Prendergast, F. G. (1991) *Biochemistry 30*, 7615−7630.
51. Persechini, A., McMillan, K., and Leaky, P. (1994) *J. Biol. Chem. 269*, 16148−16154.
52. Beechem, J. M., and Haas, E. (1989) *Biophys. J. 55*, 1225−1236.
53. Cheung, H. C. (1991) in *Topics in Fluorescence Spectroscopy* (Lakowicz, J. R., Ed.) Vol. 2, pp 128−176, Plenum Press, New York.
54. Wu, P., and Brand, L. (1992) *Biochemistry 31*, 7939−7947.
55. Lakowicz, J. R., Gryczynski, I., Laczko, G., Wiczk, W., and Johnson, M. L. (1994) *Protein Sci. 3*, 628−637.
56. Wiczk, W. M., Gryczynski, I., Szmacinski, H., Johnson, M. L., Kruszynski, M., and Zboinska, J. (1988) *Biophys. Chem. 32*, 43−49.
57. Johnson, M. L., and Faunt, L. M. (1992) *Methods Enzymol. 210*, 1−37.
58. Hühmer, A. F., Gerber, N. C., de Montellano, P. R., and Schöneich, C. (1996) *Chem. Res. Toxicol. 9*, 484−491.
59. Klee, C. B., Crouch, T. H., and Krinks, M. H. (1979) *Proc. Natl. Acad. Sci. U.S.A. 76*, 6270−6273.
60. Maune, J. F., Beckingham, K., Martin, S. R., and Bayley, P. M. (1992) *Biochemistry 31*, 7779−7786.
61. Zhang, M., Li, M., Wang, J. H., and Vogel, H. J. (1994) *J. Biol. Chem. 269*, 15546−15552.

62. Browne, J. P., Strom, M., Martin, S. R., and Bayley, P. M. (1997) *Biochemistry 36*, 9550−9561.
63. Cooper, T. M., and Woody, R. W. (1990) *Biopolymers 30*, 657−676.
64. Graddis, T. J., Myszka, D. G., and Chaiken, I. M. (1993) *Biochemistry 32*, 12664−12671.
65. Willis, K. J., Neugebauer, W., Sikorska, M., and Szabo, A. G. (1994) *Biophys. J. 66*, 1623−1630.
66. Dahms, T. E., and Szabo, A. G. (1995) *Biophys. J. 69*, 569−576.
67. Babu, Y. S., Sack, J. S., Greenough, T. J., Bugg, C. E., Means, A. R., and Cook, W. J. (1985) *Nature 315*, 37−40.
68. Craig, T. A., Watterson, D. M., Prendergast, F. G., Haiech, J., and Roberts, D. M. (1987) *J. Biol. Chem. 262*, 3278−3284.
69. Kataoka, M., Head, J. F., Persechini, A., Kretsinger, R. H., and Engelman, D. M. (1991) *Biochemistry 30*, 1188−1192.
70. Yin, D., Sun, H., Weaver, R. F., and Squier, T. C. (1999) *Biochemistry 38*, 13654−13660.
71. Gao, J., Yao, Y., and Squier, T. C. (2001) *Biophys. J. 80*, 1791−1801.
72. Kung, C. R., Preston, R., Maley, M. E., Ling, K.-Y., Kanabrocki, J. A., Seavey, B. R., and Saimi, Y. (1992) *Cell Calcium 13*, 413−425.
73. Sacks, D. B., Lopez, M. M., Li, Z., and Kosk-Kosicka, D. (1996) *Eur. J. Biochem. 239*, 98−104.
74. Barbato, G., Ikura, M., Kay, L. E., Pastor, R. W., and Bax, A. (1992) *Biochemistry 31*, 5269−5278.
75. Provencher, S. W., and Glöckner, J. (1981) *Biochemistry 20*, 33−37.
76. Provencher, S. W. (1982) *Comput. Phys. Commun. 27*, 229−242.
77. Fasman, G. D. (1996) in *Circular Dichroism and the Conformational Analysis of Biomolecules* (Fasman, G. D., Ed) pp 381−412, Plenum Press, New York.
78. Anderson, R. L. (1987) *Practical Statistics for Analytical Chemists*, pp 72−72, Van Nostrand Reinhold, New York.
79. Fairclough, R. H., and Cantor, C. R. (1978) *Methods Enzymol. 48*, 347−379.
80. Stryer, L. (1978) *Annu. Rev. Biochem. 47*, 819−846.
81. Beechem, J. M., Gratton, E., Ameloot, M., Knutson, J. R., and Brand, L. (1991) *Topics in Fluorescence Spectroscopy* (Lakowicz, J. R., Ed.) Vol. 2, pp 241−306, Plenum Press, New York.

BI0104266